https://doi.org/10.17221/159/2025-CJFS

Eco-friendly synthesis of ZnO nanoparticles for improved pectin/chitosan hydrogels with antibacterial activity

Shirin Gull[1], Huma Umbreen[1], Mahr Un Nisa[1], Abid Rashid[2]*

[1]Department of Nutritional Sciences, Government College University Faisalabad, Faisalabad, Pakistan
[2]Faculty of Medical Sciences, Government College University Faisalabad, Faisalabad, Pakistan

**Corresponding author: huma_umbreen@yahoo.com*

Citation: Gull S., Umbreen H., Nisa M.U., Rashid A. (2026): Eco-friendly synthesis of ZnO nanoparticles for improved pectin/chitosan hydrogels with antibacterial activity. Czech J. Food Sci., 44: 326–341.

Abstract: The core objective of the present study was to develop a novel nanocomposite pectin/chitosan hydrogel based on green-synthesised zinc oxide nanoparticles (ZnO NPs-L). For this purpose, zinc oxide nanoparticles were prepared by the solution casting method, using extract from aloe vera leaves, and were incorporated into pectin/chitosan hydrogels (0, 10, and 20%). The nanoparticles were analysed using scanning electron microscopy, X-ray diffraction, UV-Vis, and FTIR (Fourier transform infrared) spectroscopy. Moreover, the hydrogels were evaluated through FTIR, scanning electronic microscopy, atomic force microscopy, gel fraction, contact angle measurements, swelling ratio, investigations of thermal stability, mechanical strength and antibacterial activity. The structural heterogeneity and surface roughness of the hydrogel were evidenced by SEM analysis. The results showed that incorporation of ZnO NPs-L into hydrogel enhanced gel fraction to > 65%, surface wettability to > 64°, tensile strength to > 5.8 MPa, and swelling ratio to > 4 140 in a dose-dependent manner. Further, ZnO NPs-L (20 mg) loaded hydrogels exhibited the highest zone of inhibition against *Escherichia coli* (> 13 mm) and *Staphylococcus aureus* (> 12 mm). The findings suggested that pectin/chitosan/ZnO NPs-L hydrogels have appropriate mechanical flexibility, swelling behaviour and antibacterial activities, which are required for their effective use in the biomedical and agricultural sectors.

Keywords: green nanotechnology; aloe vera extract; biopolymer matrix; nanocomposites; biomaterials

With recent developments in the field of material science, the demand for the development of functional biopolymers has increased to replace plastics. In this regard, hydrogels derived from natural biopolymers, particularly polysaccharides have gained significant attention due to their renewability and biodegradability, surpassing the attributes of synthetic polymer-based hydrogels. Among polysaccharides, chitosan (CS) and pectin (PT) are particularly important in the formation of bio-hydrogels due to their higher water-holding capacity and stronger gel-forming ability (Qureshi et al. 2024). Since both are approved as safe to use in food and pharmaceutical products, their composites offer a broad spectrum of applications in agricultural biotechnology as carriers for pesticides or seed coatings that degrade into nutrients (Popa et al. 2025). However, pure hydrogels lack the necessary durability and antifungal 'punch' required to prevent crop spoilage and soil-borne diseases (Yadav et al. 2022).

To overcome these physical and biological deficiencies, researchers have turned towards the incorporation of inorganic nanofillers to create nanocomposite

Supported by the Department of Nutritional Sciences, Govt. College University Faisalabad, Pakistan.

https://doi.org/10.17221/159/2025-CJFS

hydrogels. Among these, ZnO nanoparticles (NPs) stand out due to low cytotoxicity, higher antimicrobial activity, and a high surface area to volume ratio, which enhances the mechanical toughness of the polymer matrix (Alameen et al. 2024). However, the usual methods used for the formation of ZnO NPs rely on chemical reducing agents, which may have toxic outcomes and may cause cytotoxic effects in the final product, such as hydrogel, thus making them hazardous to agriculture, health and the environment (Kumar et al. 2021). The present study offers a green synthesis method based on the use of aloe vera leaf extract for the formulation of nanoparticles. Aloe vera is one of the most renowned medicinal plants recognised as a miraculous gift of nature (Kaur and Bains 2023). Moreover, its rich composition of bioactive compounds has made it valuable in various fields, including the food industry, cosmetics and health care (Bhavikatti et al. 2025). The compounds present in aloe vera act as natural reducing and capping agents in the formation of nanoparticles (Ahmad and Reddy 2020). In this way, the current strategy not only eradicates the need for hazardous chemicals but also enhances the biocompatibility of the ZnO NPs. By incorporating these green nanoparticles into a PT/CS hydrogel, a synergistic material is synthesised.

Although the major emphasis of such nanocomposites has been biomedical (such as wound healing and tissue engineering), there is a need to find out their agricultural potential to ensure food security. The 'One Health' concept proposes that the structural and antimicrobial characteristics, which are needed for wound healing on the human skin, are also important in the protection of plant materials (Singh et al. 2021). In the agriculture sector, such hydrogels pave a way toward smart edible coatings to prevent post-harvest losses of fruits through protection from microbes by ZnO NPs-based pectin/chitosan matrix, which also provides a gas barrier to slow ripening (Diez-Pascual and Diez-Vicente 2014). Moreover, as zinc is an essential plant micronutrient, these biodegradable hydrogels can function as nano-fertiliser carriers, providing a controlled release of Zn into the soil without the environmental toxicity associated with chemically synthesised particles (He et al. 2020).

ZnO NPs have the potential to form polymer nanocomposites that can be used in food packaging due to their ability to enhance mechanical strength and controlled release (Pires et al. 2023). The antimicrobial properties and excellent UV-blocking properties have made zinc oxide a promising nanofiller due to its cost-effectiveness, higher antimicrobial activity, and UV-blocking properties. ZnO has been registered by the US Food and Drug Administration (FDA) in the Generally Recognised as Safe (GRAS) list, so it is edible (Boura-Theodoridou et al. 2020). In addition, these bio-nanocomposites are aimed at enhancing the performance of the general food packaging properties, i.e. barrier properties, mechanical strength and thermal stability. Further, these can be added to food items as bacteriostatic agents, antioxidants, plant extracts and enzymes to increase the shelf-life of the food products (Youssef and El-Sayed 2018). Moreover, in the food packaging industry, hydrogels are used as absorbent pads and as biodegradable, antimicrobial and antioxidant packaging (Karanth et al. 2023).

Despite the benefits provided by chitosan, pectin, and ZnO individually, there exists a prominent research gap regarding the use of aloe vera-mediated ZnO in a dual-polysaccharide hydrogel for multisectoral applications. The present study addresses this gap by characterising a multifunctional pectin/chitosan/ZnO nanocomposite hydrogel. By assessing its physicochemical properties and antibacterial performance, this research shows the versatility of eco-friendly nanotechnology in bridging the gap between clinical therapeutics and sustainable agri-food systems.

MATERIAL AND METHODS

Materials

Pectin (Mw = 381.042 g·mol^{-1}; DDA = 92%) and chitosan (CS) (Mw = 3.03 × 10^6 g·mol^{-1}; viscosity = 700 cp; DDA = 90%) were sourced from Merck (Germany). Chemicals such as carbon tetrachloride (CCl_4), silver nitrate ($AgNO_3$), zinc acetate dehydrate [$Zn(CH_3CO_2)_2$], sodium hydroxide (NaOH), and chromic acid (H_2CrO_4) were acquired from Sigma Aldrich (USA). Double-distilled water was utilised for all solution preparations. Additionally, $CaCl_2$, NaOH, and acetic acid (99%) were procured from Merck (Germany).

Plant extract preparation

For plant extract preparation, 20 g of finely chopped aloe vera (AV) leaves were mixed in 100 mL of distilled water. The mixture was stirred for 10 min at 60 °C using a hot plate stirrer at 500 rpm (HTS-1003, LMS, Japan). The solution was allowed to cool down to room temperature and then was filtered through vacuum filtration and used for the synthesis of zinc oxide nano particles [ZnO NPs-L (leaves)] (Nejatzadeh-Barandozi 2013).

https://doi.org/10.17221/159/2025-CJFS

Synthesis of ZnO NPs-L

For the preparation of ZnO NPs-L using AV plant extracts, 3 g of zinc acetate dihydrate were dissolved in 50 mL of water and stirred at room temperature for one hour using a magnetic stirrer (MS4-H380-E, Biobase, China) (Mahendiran et al. 2017). Gradually, 20 mL of 10% NaOH solution was added to it while stirring. Afterwards, added 50 mL of plant extract, covered the flask, and let it set for one hour. Placed the mixture on an orbital shaker at 100 rpm for four hours. Let the solution stand for 30 min, during which yellow-coloured ZnO NPs-L settled at the bottom. Separated the ZnO NPs-L by centrifugation and carefully decanting the supernatant. Finally, the sample was dried for two hours in an oven at 80 °C (Meji et al. 2023; Rata et al. 2023; Dzulkharnien et al. 2024).

Preparation of hydrogels

Initially, 0.5 g of pectin was dissolved in deionised water (50 mL) in a beaker and stirred at 60 °C until fully dissolved, forming a clear solution. At the same time, 0.5 g of chitosan was dissolved in 2% acetic acid (50 mL) under magnetic stirring at 60 °C in another beaker. The PT solution was then blended with the CS solution and was further stirred continuously for 2 h. ZnO NPs-L were added to the CS/PT blend and mixed for an additional hour. The resulting solution was carefully poured into petri dishes and subsequently dried at 50 °C in a vacuum drying oven. Three formulations were prepared using this method, with varying concentrations of ZnO NPs-L: PC (without ZnO NPs-L), PCL-1 (10 mg ZnO NPs-L), and PCL-2 (20 mg ZnO NPs-L) (Sabbagh et al. 2023; Rastegari et al. 2023).

Characterisation

UV-visible spectroscopy. The UV-Vis spectra of ZnO nanoparticles (ZnO NPs-L) were obtained using a UV-Vis spectrometer (BK-UV1800PC, Biobase, China) over a wavelength range of 200–600 nm. The samples were dispersed and diluted in double-distilled water under ambient conditions before measurement (Kamanna et al. 2023).

Fourier transform infrared spectroscopy (FTIR). The FTIR spectroscopy was performed to analyse ZnO nanoparticles (ZnO NPs-L) and hydrogel composite samples (IR Prestige-21; Shimadzu, Japan). An FTIR spectrophotometer with a horizontal attenuated total reflectance (HATR) accessory featuring zinc selenide (ZnSe) crystal was used. The spectrum was noted at a resolution of 4.0 cm^{-1} over a scanning range of 4 000 to 650 cm^{-1}, using air background as the reference (Pathan and Bose 2020).

Xray diffraction (XRD). The X-ray diffraction was conducted to determine the phases and crystallinity using an X-ray diffractometer (Equinox 2000, Thermo Scientific, USA). The analysis was conducted using Cu Kα radiation (λ = 1.54 Å), and the 2θ scanning ranged from 20° to 80° (Gojova et al. 2007). The crystallite size (D) was estimated by the Debye-Scherer equation as follows:

$$D = K\lambda / \beta \cos(\theta) \quad (1)$$

where: K – shape factor; λ = 1.5406 Å; β – full width at half maximu; θ – Bragg angle of the peak 2θ (Ebrahimi et al. 2018).

Morphological assessment

Scanning electron microscopy (SEM). The ZnO NPs-L and hydrogel composite samples were examined using a scanning electron microscope (Cube 10 Emcraft, Hanam, Republic of Korea) for surface analysis. The samples underwent sputter coating with a thin layer of gold for 120 s, which lessened charging effects during examination to improve imaging quality (Wang et al. 2020). SEM image was used to determine the particle size distribution of ZnO NPs-L with the ImageJ software (version 1.54 g).

Atomic force microscopy (AFM). AFM was performed using an atomic force microscope (Xe7, Park Systems, Republic od Korea) to attain topographical images of the hydrogel surfaces. The surface roughness was analysed over a 5 × 5 μm scan area in contact mode, with an oscillating tip for precise measurement (Xue et al. 2021).

Thermogravimetric analysis. Thermal stability of the hydrogel composite was evaluated using a thermogravimetric analyser (409C, NETZSCH, Germany). Samples were heated at the rate of 10 °C per min in a range of temperatures from 0 to 600 °C under N_2 gas with a flow rate of 15 $mL \cdot min^{-1}$ (Cao et al. 2019).

Mechanical stability. The samples of the hydrogels were tested for mechanical stability using a Tensile Testing Machine (STM-1, Santam Engineering Design Co., Iran) according to the ASTM D882-02 standard. The prepared hydrogel composite samples were cut into strips measuring 4 × 1 cm with a thickness of 0.3 cm and were placed into an apparatus for stability analysis (Pathan and Bose 2020).

Gel fraction. The cross-linking of the PT/CS hydrogel composite samples was assessed with slight changes to the standard procedure. The samples were put

https://doi.org/10.17221/159/2025-CJFS

in 500-mesh stainless steel porous bags and were dried in an oven (BOV-TC, Biobase, China) at 40 °C until a constant weight was achieved. Fully dried samples were placed in a Soxhlet apparatus, where distilled water was used as a solvent to separate the cross-linked materials, and were processed for 40 h (Seliktar 2012).

The gel content was then determined by following the equation as follows:

$$Gel\ fraction\ (\%) = W1/W2 \times 100 \quad (2)$$

where: $W1$ – the weight of the hydrogel after oven drying; $W2$ – the initial weight of the dried hydrogel.

Contact angle. The hydrophilicity of the prepared PT/CS-based hydrogel composite was determined by contact angle. For this estimation, samples were positioned on microscope slides and were inverted in a container filled with distilled water. To measure the water in the dry hydrogel film interface, a goniometer (Kernco Instrument Co. Inc., USA) was used. A droplet of distilled water, using a syringe, was carefully applied to the hydrogel sample, and the contact angle was measured from both sides of the droplet (Fu et al. 2017; Multanen and Bhushan 2019; Zhao et al. 2021).

Swelling experiments

The equilibrium swelling condition was obtained by immersing the hydrogel samples in the medium and measuring their weight at regular time intervals until no further change in weight was observed, indicating that equilibrium had been reached.

Swelling behaviour of hydrogel in distilled water. Pre-weighed hydrogel samples were immersed in distilled water to evaluate the swelling behaviour. At specified time intervals, samples were taken out and blotted with filter paper to remove any excess water. The swollen weight of the hydrogel samples was then measured (Multanen and Bhushan 2019). The swelling percentage was determined using the following equation:

$$Swelling\ (\%) = W_{sg} - W_{dg}/W_{dg} \times 100 \quad (3)$$

where: W_{dg} – the weight of the dry gel; W_{sg} – the weight of the swollen gel.

Swelling index of hydrogel in buffer solutions. To evaluate swelling in different buffer solutions, buffers at a range of pH levels (2, 4, 6, 7, 8, and 10) were prepared according to standard procedures. Pre-weighed prepared samples were immersed in buffer solutions in Petri dishes and allowed to equilibrate. After equilibration was achieved, the buffer solutions were removed from the Petri dishes, and the samples were gently blotted with a filter paper to remove the excess solution. The weight of swollen hydrogels was measured, and the degree of swelling was calculated using Equation 3 (Ko et al. 2010).

Swelling analysis of hydrogels in electrolyte solutions. To measure swelling behaviour in ionic solutions, NaCl and $CaCl_2$ solutions with different molarities (0.1, 0.3, 0.5, 0.7, and 0.9 M) were prepared according to standard protocols. Pre-weighed hydrogel samples were separately engrossed in these electrolyte (ionic) solutions until reaching an equilibrium. After the equilibrium was achieved, the samples were gently blotted with a filter paper to wipe out the surface droplet. The swelling ratio was evaluated as described in Equation 3 (Ko et al. 2010). This process was repeated three times for each sample.

In vitro antimicrobial analysis. The experiment aimed to determine the antibacterial effects of prepared hydrogels on two bacterial strains: *Staphylococcus aureus and Escherichia coli.* An antibacterial assay was performed in triplicate to measure the effect of ZnO NPs-L concentrations (Ramanan et al. 2017). Chloramphenicol was used as a positive control, and 1 mL DMSO served as a negative control. The zones of inhibition were measured using the disk diffusion technique. Discs infused with hydrogels were placed on agar plates inoculated with the bacterial strains, and the plates were incubated at 37 °C overnight. The presence of a zone of inhibition around the disc after incubation showed the existence of antibacterial activity (Pellegrin et al. 2018).

Statistical analysis

Analyses where possible were performed in triplicate, and values were expressed as a mean along with standard deviation using SPSS software (version 18, IBM SPSS, USA). The results were checked for significant difference using one-way ANOVA at $P \leq 0.05$. The Fourier-transform infrared (FTIR), X-ray diffraction, and scanning electron microscope data were processed and analysed using Origin software (OriginLab Corporation, Northampton, USA) for baseline correction, peak fitting, graphical representation, and ImageJ software 15.4 g.

RESULTS AND DISCUSSION

UV-Vis spectrum analysis

The UV-Vis spectrum of ZnO NP-L, synthesised using 20 mL of aloe vera extract, provides key insights into the optical properties of the NPs. Normally, near 300–450 nm, ZnO NPs-L show absorption and confirmation in the UV

https://doi.org/10.17221/159/2025-CJFS

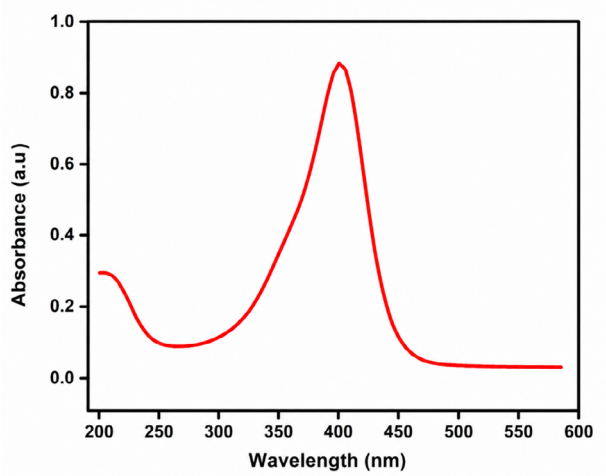

Figure 1. UV-Vis spectrum of zinc oxide nano particles (ZnO NPs-L)

region, and the specific wavelength of the absorption peak can be influenced by factors such as the shape and size of the NPs, which are affected by the concentration of AV extract used in the preparation of nanoparticle synthesis (Li et al. 2010). The narrow peak proves the purity and conformation of the ZnO NPs-L (Figure 1).

FTIR analysis

The FT-IR spectra of ZnO NPs-L nanoparticles synthesised from leaf hydrogel composites are illustrated in Figure 2A–2C. FTIR spectroscopy was used to identify the functional groups. Metal oxides typically display absorption bands in the fingerprint region below 600 cm^{-1} due to interatomic vibrations. In the present study, absorption bands observed around 650 cm^{-1} are attributed to ZnO stretching vibrations, confirming the successful formation of ZnO NPs-L. The green synthesised ZnO NPs-L show a band at 3 385–3 413 cm^{-1}, corresponding to the broadening vibrations of O-H groups. The bands at 2 834 cm^{-1} and 2 940 cm^{-1} correspond to the symmetric and asymmetric C-H vibrations of aliphatic groups. Sharp absorption peaks observed between 1 700 and 1 600 cm^{-1} are attributed to C=O stretching of carbonyl or amide groups and N-H bending vibrations, while peaks in the 1 400–1 480 cm^{-1} range correspond to aromatic C=C stretching and amide II vibrations originating from bioactive compounds present in the leaf extract (Aziz et al. 2019). The absorption band observed near 1 020 cm^{-1} is assigned to C-O-C and C-O stretching vibrations of polysaccharide units in the polymer matrix, rather than Zn-O bonding. These assignments are consistent with reported FTIR spectra of chitosan and related biopolymers (Li et al. 2018). The broad band between 3 490 and 3 120 cm^{-1} further supports the presence of O-H groups in PT, CS, and ZnO NPs-L, as well as amino groups present in CS and ZnO NPs-L (Pellegrin et al. 2014). The broadness of this band suggests

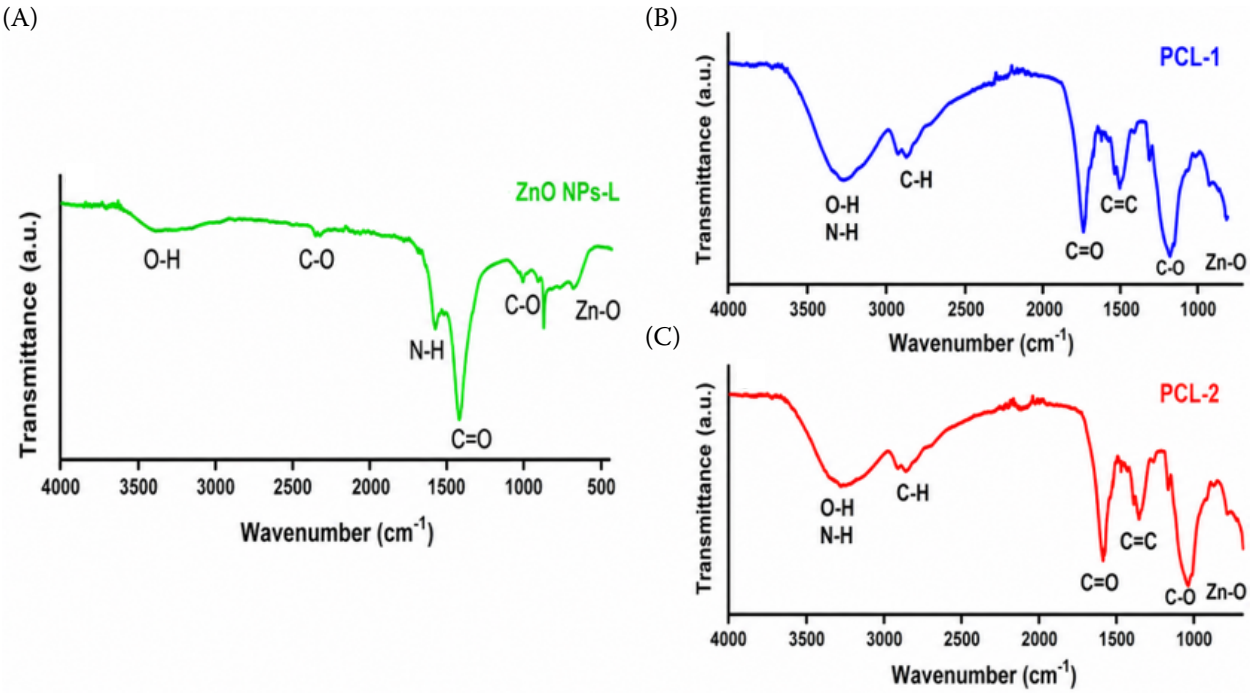

Figure 2. Fourier transform infrared spectroscopy (FTIR) spectra of (A) zinc oxide nanoparticles (ZnO NPs-L), (B) hydrogel sample: PCL-1 and (C) hydrogel sample: PCL-2

PCL-1 – hydrogel with 10 mg ZnO NPs-L; PCL-2 – hydrogel with 20 mg ZnO NPS-L

https://doi.org/10.17221/159/2025-CJFS

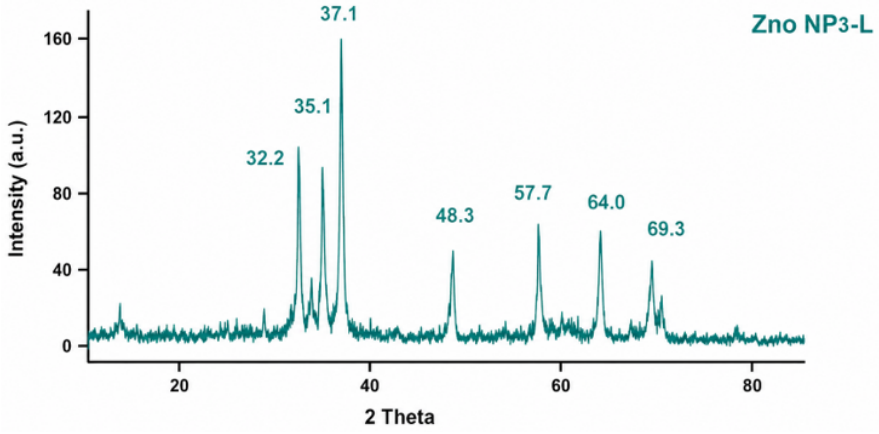

Figure 3. X-ray diffraction (XRD) spectrum of zinc oxide nanoparticles (ZnO NPs-L)

hydrogen bonding between the OH^- and NH^{2+} groups of polymer chains and ZnO NPs-L. The band observed at 1 612–1 730 cm^{-1} corresponds to the carbonyl group in the reaction medium (Pellegrin et al. 2014). Overall, the FTIR results confirm the successful incorporation of ZnO NPs-L within the polymer matrix through physical interactions without altering the fundamental chemical structure of the polymers.

X-ray diffraction

The XRD pattern shown in Figure 3 represents the crystalline structure of ZnO nanoparticles (ZnO NPs-L). The hexagonal crystal structure of the nanoparticles is confirmed by planes of ZnO, which are observed as diffraction peaks at 2θ values of 32.3, 37.0, 48.5, 57.6, 64.1, 69.4 and 91.4°. The intense and sharp peaks confirmed that the synthesised ZnO NPs-L are highly crystalline (Hua et al. 2017). The peak at 37.0° is particularly prominent, suggesting that the NPs have a preferred orientation along this plane, which is usually noticed in ZnO NPs synthesised using green methods. The AV leaf extract served as a reducing agent and as a capping agent, which helped in controlling the size and morphology of the NPs, contributing to their crystalline nature. The XRD pattern is consistent with the standard ZnO crystal structure, indicating the successful synthesis of pure ZnO NPs-L without any significant impurities. The crystallite size (D) was estimated by the Debye-Scherrer equation (Equation 1, Tian et al. 2020). The Debye-Scherrer equation calculated the crystallite size as 34 nm.

Surface morphology

Scanning electron microscopy. The SEM images of AV-based ZnO NPS-L (Figure 4A–4C) confirmed

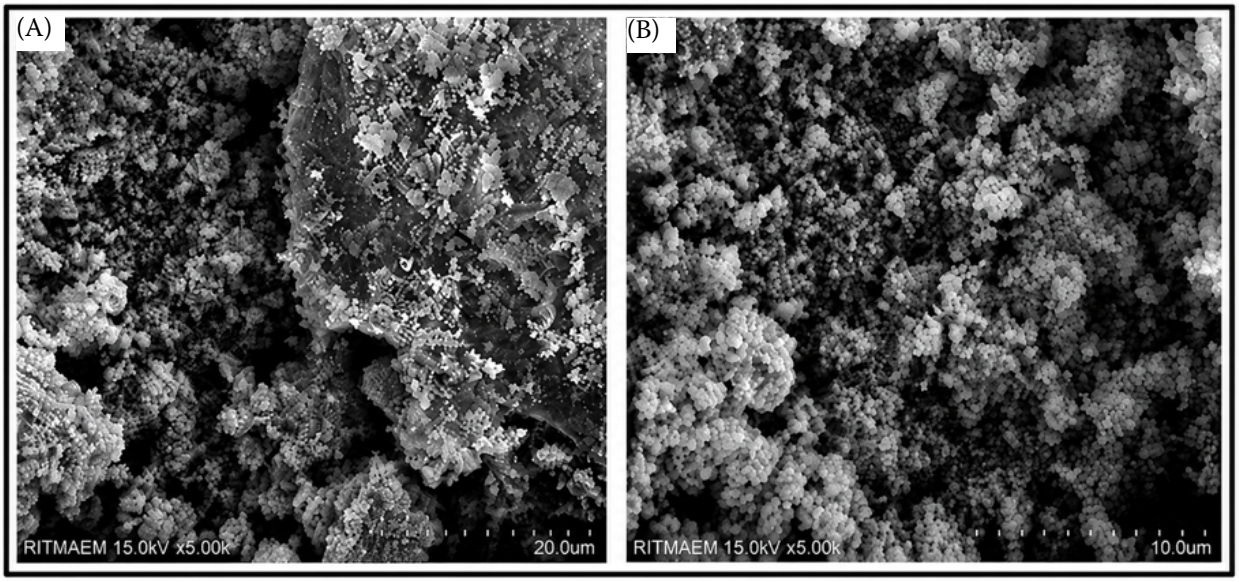

Figure 4. Scanning electron microscopy (SEM) images of ZnO nanoparticles (ZnO NPs-L) at different magnification: (A) 200k× and (B) 500k×

https://doi.org/10.17221/159/2025-CJFS

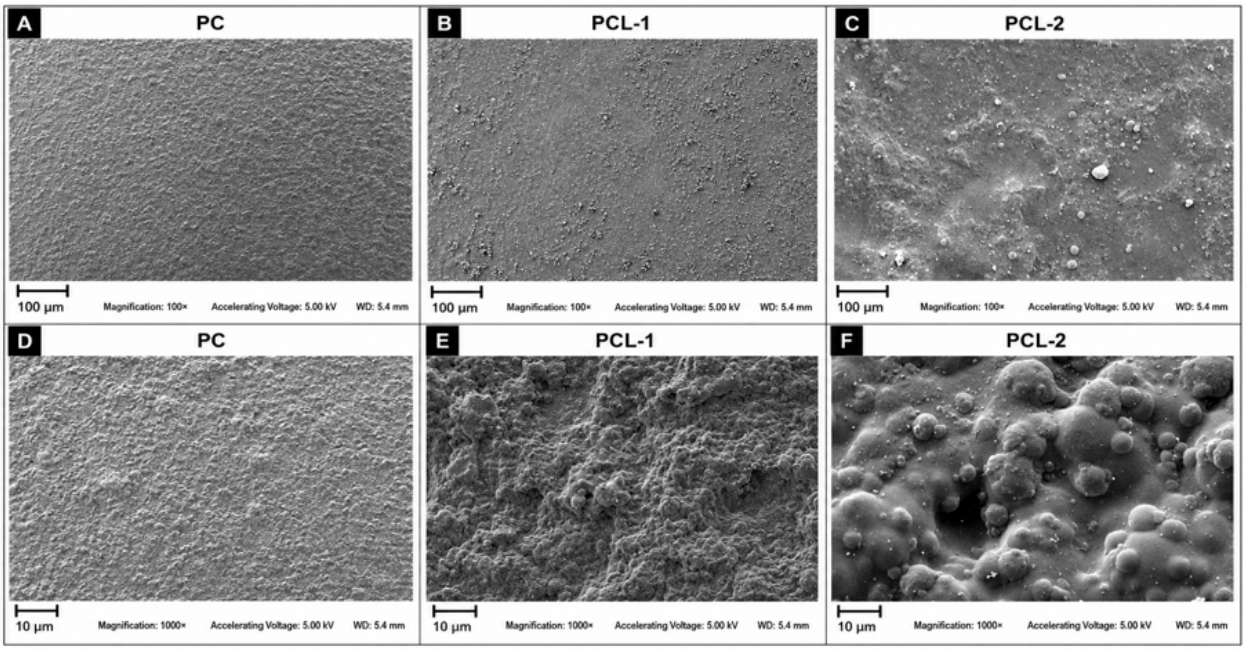

Figure 5. Scanning electron microscopy (SEM) images of PT/CS based hydrogels as PC (without ZnO NPs-L), PCL-1 (10mg ZnO NPs-L) and PCL-2 (20 mg ZnO NPs-L at different magnification (100×, 300k×)

PT – pectin; CS – chitosan; ZnO NPs-L – zinc oxide nanoparticles

irregular, porous and heterogeneous surface morphologies. A sponge-like structure with spherical air bubbles was also detected by SEM in ZnO NPS-L. The SEM images revealed that NPs appeared to be aggregated into clusters, which contribute to high surface area and consequently are beneficial for applications in biomedicine and the agriculture sector (Ahmad and Reddy 2020).

Moreover, the surface morphology of PT- and CS-based hydrogels containing ZnO NPs-L with AV leaf extracts is shown in Figure 5. The control sample (PC) exhibited a relatively smooth and uniform surface with minor texturing. In contrast, the hydrogel with a low concentration of ZnO NPs-L displayed a rougher surface with pronounced texturing and small particle-like formations. The hydrogel with a higher concentration of ZnO NPs-L (PCL-2) showed the roughest and most irregular surface, with significant texturing and larger particle clusters. The increased surface roughness and heterogeneity in PCL-1 and PCL-2 indicate the successful incorporation of ZnO NPs-L particles, which are expected to enhance the hydrogels' mechanical properties, swelling behaviour and functional performance in various applications (Smeraldi et al. 2017). The samples were analysed with a histogram shown in Figure 4C. The histogram indicates a narrow and monodisperse distribution, where the majority of the particles are within the 135–140 nm range. The positive skewness implies uniform nucleation and a certain level of variation in particle growth, which is characteristic of green synthesis. This homogeneity of scale is useful to antimicrobial applications, in which a fixed surface area and reactivity are important. The narrowing distribution also indicates that the phytochemicals in the plant extract utilised in the synthesis are effective capping and stabilising agents (Momoh et al. 2024).

Atomic force microscopy. Figure 6 exhibits the three-dimensional AFM images of hydrogel composite samples with varying weight percentages of ZnO NPs-L. The surface topography shows significant differences in surface roughness among the prepared hydrogel samples. The hydrogel (PC) revealed a relatively smoother surface with a root mean square (RMS) value of 145.31 nm. In contrast, by structural modifications, the hydrogel with 10 mg ZnO NPs-L (PCL-1) showed increased surface roughness at 167.37 nm, while the hydrogel containing 20 mg ZnO NPs-L (PCL-2) exhibited the highest roughness at 278.15 nm, and the higher roughness contributes to the enhancement of the interface. In the membrane images, surface depressions appear darker, while elevations indicate variations in brightness. Bright areas indicate protrusions on the hydrogel surface, whereas shadowy regions show, in some cases, pores or valleys. The gradually increased roughness corresponds to enhanced zinc particle deposition, which is effective in enhancing the capacity

https://doi.org/10.17221/159/2025-CJFS

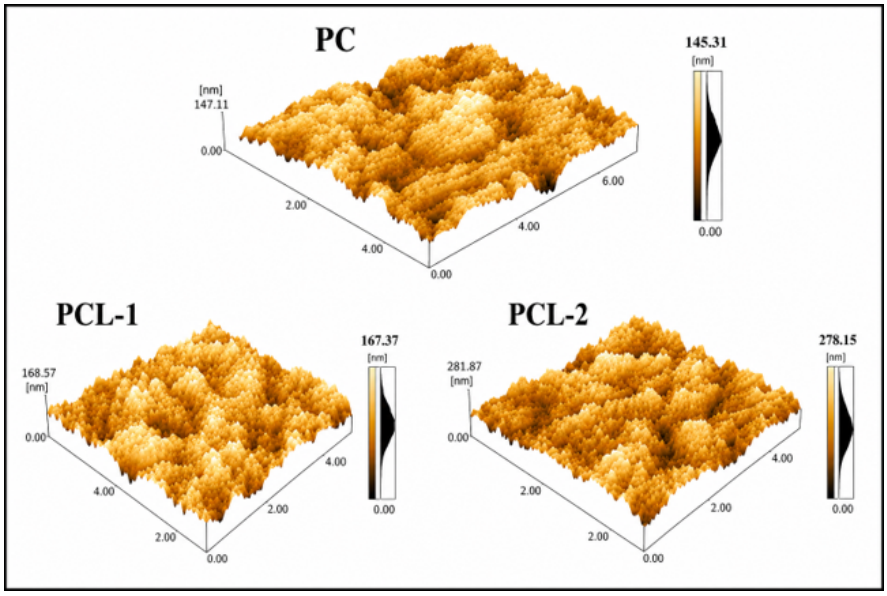

Figure 6. Atomic force microscopy (AFM) images of PT/CS based hydrogels as PC (without ZnO NPs-L), PCL-1 (10 mg ZnO NPs-L) and PCL-2 (20 mg ZnO NPs-L)

PT – pectin; CS – chitosan; ZnO NPs-L – zinc oxide nano particles

of the hydrogel to trap water within the hydrogel matrix (Lee et al. 2017). This roughness increased the surface area, thus supporting interaction between surface hydroxyl groups and water and improving hydrophilicity. These changes in surface morphology are crucial for optimising hydrogel applications in biomedical and agricultural applications (Rhodes 2015).

Gel content. Figure 7 exhibits the effect of ZnO NPs-L on gel content variation. The control sample exhibits a lower gel content compared to other samples. The gel content increased with an increase in the concentration of ZnO NPs-L in a dose-dependent manner from PCL-1 to PCL-2. The results also validate the effectiveness of ZnO NPs-L, as it forms van der Waals forces, hydrogen bonds, and coordination bonds, which collectively strengthen the network structure (Ahmad et al. 2008).

The contact angle measures the hydrophilic polymeric network of the hydrogel. In literature, a contact angle ranging from 0° to 90° indicates the hydrophilic nature of a material (Read et al. 2011). The contact angles measured for all hydrogels were within this range, confirming the hydrophilic properties of the hydrogel material. Incorporation of ZnO NPs-L into

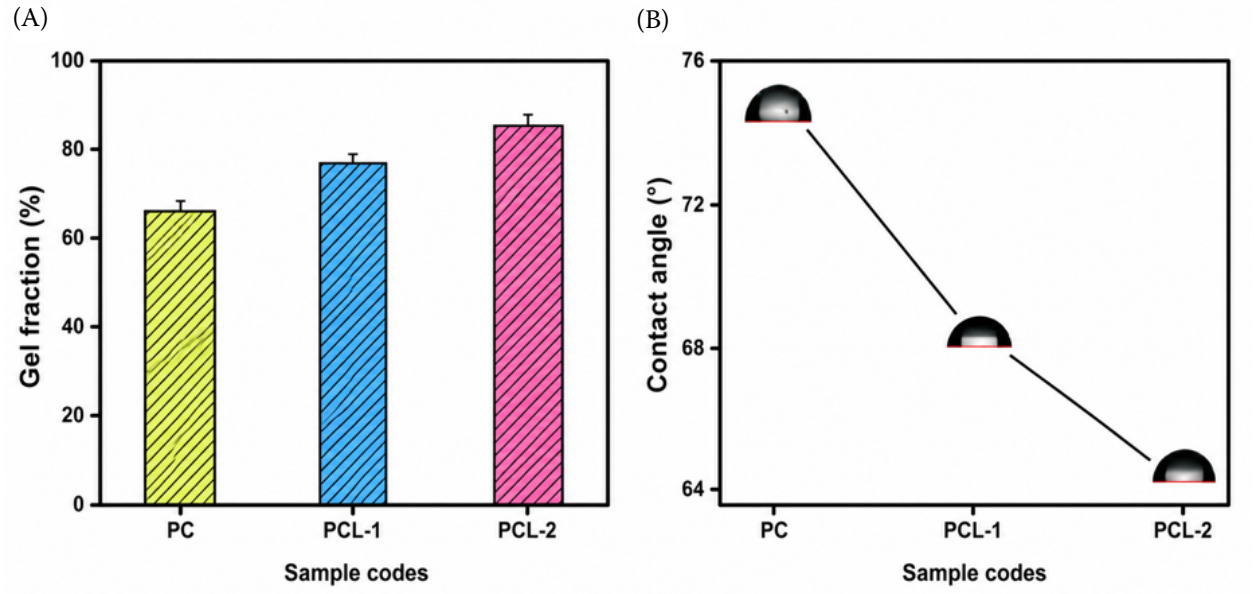

Figure 7. (A) Gel content and (B) contact angle of PT/CS hydrogels with and without ZnO NPs-L

PT – pectin; CS – chitosan; ZnO NPs-L – zinc oxide nano particles; PC – hydrogel without ZnO NPs-L; PCL-1 – hydrogel with 10 mg ZnO NPs-L; PCL-2 – hydrogel with 20 mg ZnO NPs-L

https://doi.org/10.17221/159/2025-CJFS

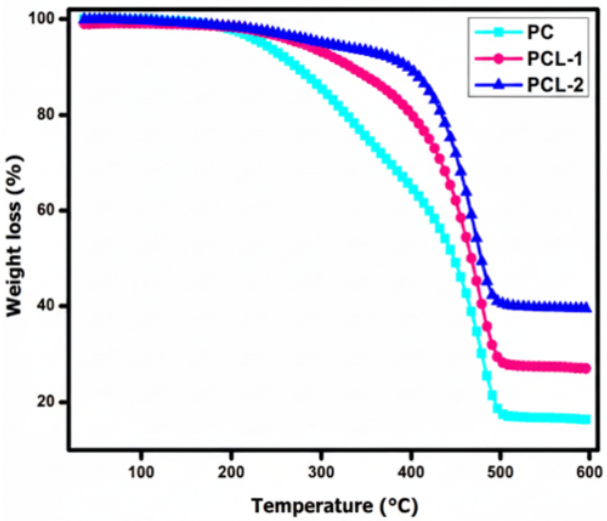

Figure 8. Thermogravimetric analysis (TGA) thermograms of PC (hydrogel without ZnO NPs-L), PCL-1 (hydrogel with 10 mg ZnO NPs-L) and PCL-2 (hydrogel with 20 mg ZnO NPs-L)

ZnO NPs-L – zinc oxide nanoparticles

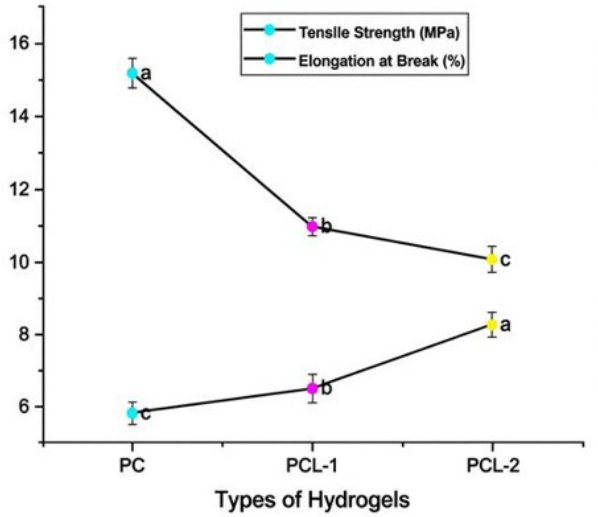

Figure 9. Elongation at break (%) and tensile strength (MPa) of PT/CS based hydrogels as PC (without ZnO NPs-L), PCL-1 (10mg ZnO NPs-L) and PCL-2 (20 mg ZnO NPs-L)

PT – pectin; CS – chitosan; ZnO NPs-L – zinc oxide nanoparticles

hydrogels significantly influenced their surface wettability, as shown by contact angle measurements. The pure hydrogel (PC) showed the maximum contact angle, indicating the minimum hydrophilic surface. In contrast, hydrogels with 10 mg (PCL-1) and 20 mg (PCL-2) of NPs showed progressively lower contact angles, demonstrating more hydrophilicity, as shown in Figure 7B. This improvement in wettability due to increased NP concentration is explained by the hydrophilicity of ZnO, and such modified hydrogels are in demand in the biomedical and agriculture fields (Ngo and Natowitz 2018).

Thermogravimetric analysis (TGA). TGA was performed to evaluate the thermal stability of the PT/CS-based hydrogels. All the hydrogels showed three steps of weight loss during thermal degradation. The initial minimal weight loss was seen at temperatures below 100 °C and is due to the evaporation of physically absorbed water. A significant weight loss occurred between 200 °C and 450 °C, corresponding to the thermal decomposition of the main polymer matrix or organic material. The temperature range of 450 to 500 °C marks the final stage of degradation, attributed to the thermal breakdown of the hydrogel, with ash content remaining after 500 °C. Thermal analysis exhibited that all hydrogels showed a similar degradation pattern. The hydrogel with a low concentration of ZnO NPs-L (PCL-1) exhibited a similar initial weight loss pattern but demonstrated enhanced thermal stability with a smaller weight loss in the primary decomposition range, as shown in Figure 8. The hydrogel with a high concentration of ZnO NPs-L (PCL-2) showed the highest thermal stability, with a further reduced weight loss in the same temperature range. The increased thermal stability in PCL-1 and PCL-2 can be attributed to the stabilising properties of ZnO NPs-L and the reinforcing effect. The residue at 600 °C for PC, PCL-1, and PCL-2 was 26.93, 33.07, and 39.52%, respectively, representing the quantity of inorganic content. The final residues of PCL-1 and PCL-2 were higher than those of the PC, which was primarily due to the incorporation of ZnO NPs-L. These results suggest that the incorporation of ZnO NPs-L significantly improves the thermal stability of the hydrogels, which suggests its potential benefits for use in agriculture and biomedicine (Dimitrou et al. 2024).

Mechanical properties. Mechanical testing was used to evaluate the elasticity and strength of the hydrogels of PT/CS (Gila-Vilchez et al. 2019). Figure 9 shows that the tensile strength (TS) of all hydrogels' values increased with higher concentrations of ZnO NPs-L, while the elongation at break decreased accordingly (Phadke et al. 2012). The pure hydrogel (PC) showed the lowest tensile strength as compared to ZnO NPs-L incorporated hydrogels. The control sample showed 5.8 MPa strength, and PCL-1 showed 6.5 MPa, which increased to 8.3 MPa for PCL-2. However, the elongation at break for PC was 15.2%, which decreased to 10.1% for PCL-2.

https://doi.org/10.17221/159/2025-CJFS

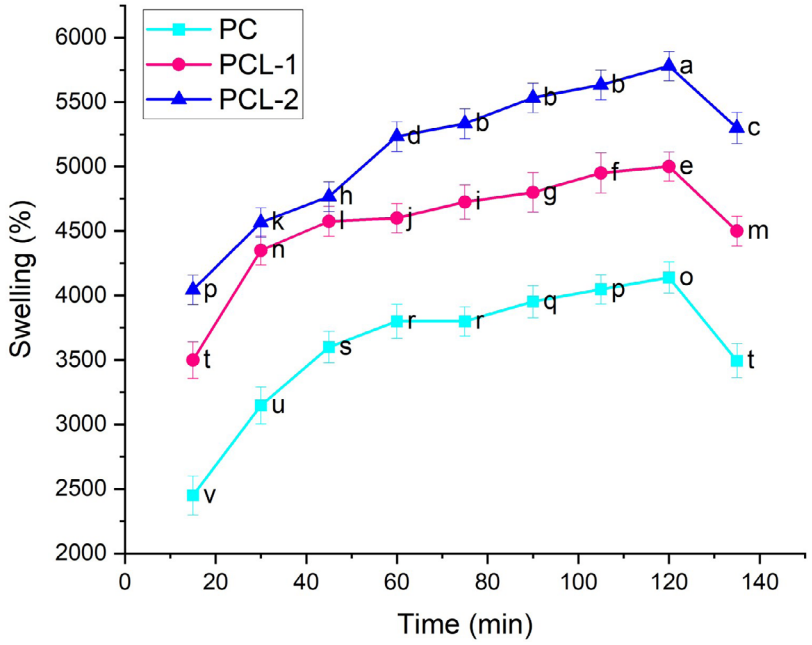

Figure 10. Swelling ratio of PT/CS based hydrogels as PC (without ZnO NPs-L), PCL-1 (10mg ZnO NPs-L) and PCL-2 (20 mg ZnO NPs-L)

PT – pectin; CS – chitosan; ZnO NPs-L – zinc oxide nanoparticles

The increase in TS and decrease in elongation at break indicate a good blending of all polymer components, which provide a rigid structure to the ZnO NPs-L incorporated hydrogels with enhanced mechanical properties. This enhancement is attributed to the reinforcing effect of ZnO NPs-L, which improves the hydrogel matrix (Zumbuehl et al. 2007). For evaluating edible films, tensile strength and elongation at break are important parameters. Tensile strength is the greatest stress the film can withstand before breaking, while elongation at break shows stretching without breaking. Both the tensile strength and elongation rely on the material's composition; the greater its elongation, the better the film's flexibility and capability to envelop wrapping food (Cheang et al. 2025).

Swelling experiments

Swelling experiments were carried out to determine the swelling capacity of hydrogels and to evaluate the impact of varying amounts of ZnO NPs-L on their

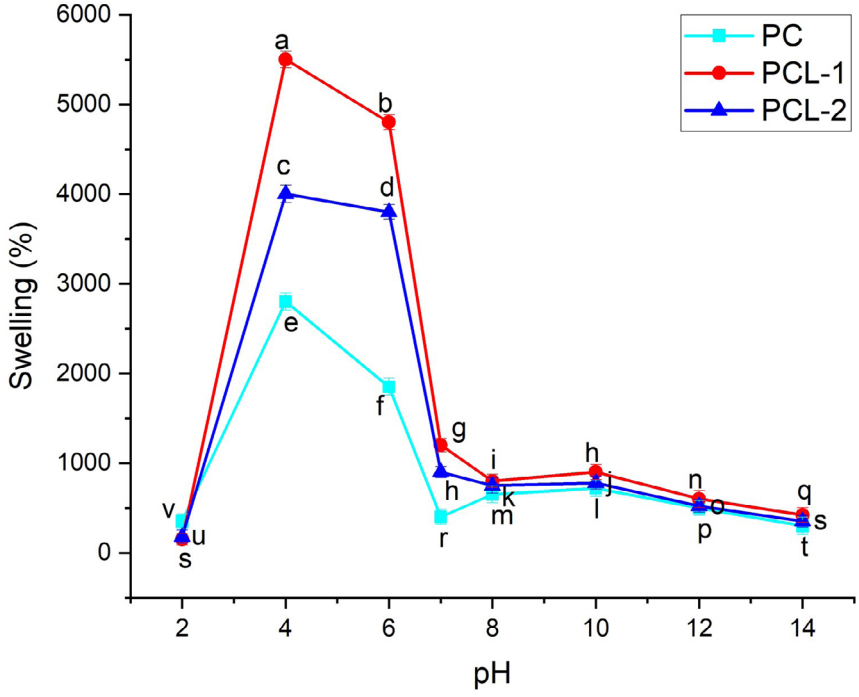

Figure 11. pH-dependent behaviour of PT/CS based hydrogels as PC (without ZnO NPs-L), PCL-1 (10 mg ZnO NPs-L) and PCL-2 (20 mg ZnO NPs-L)

PT – pectin; CS – chitosan; ZnO NPs-L – zinc oxide nanoparticles

https://doi.org/10.17221/159/2025-CJFS

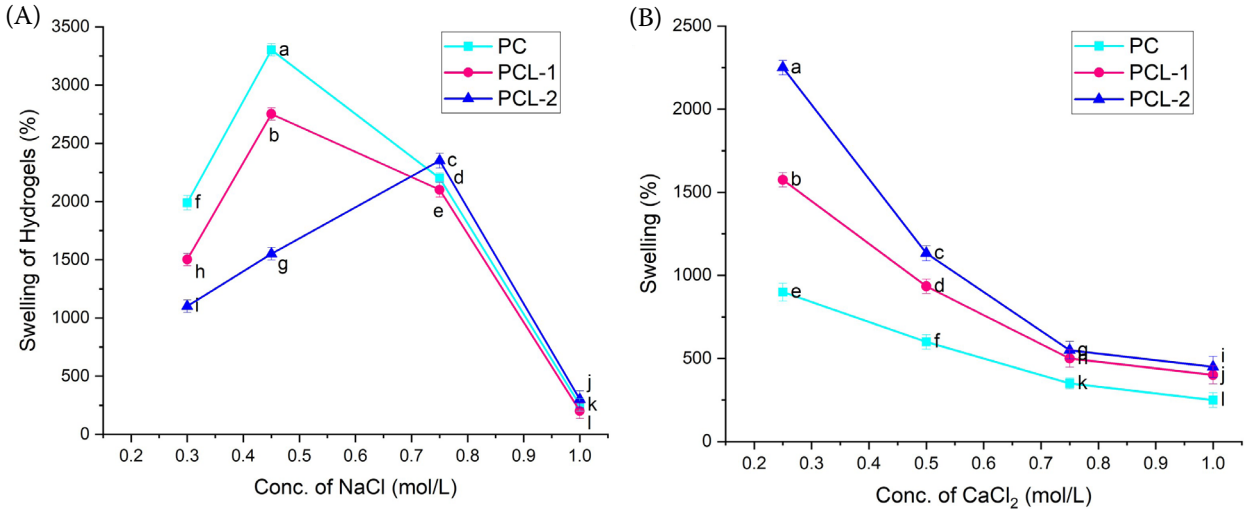

Figure 12. Effect of electrolytes on hydrogel swelling: (A) NaCl and (B) $CaCl_2$

swelling behaviour in different media, including water and salt solutions. Additionally, the pH responsiveness of these hydrogel samples was examined.

Hydrogel swelling behaviour in distilled water. Figure 10 shows the results of swelling investigations. Generally, an increase in ZnO NPs-L concentration correlates with a greater swelling capacity. For the control hydrogel (PC), swelling gradually increased until equilibrium was reached at 120 min, with a maximum swelling of approximately 4 140%. PCL-1, which contains 10 mg ZnO NPs-L, exhibited a higher swelling rate than the control, achieving a maximum swelling of 5 780% at the same equilibrium time of 120 min (Zumbuehl et al. 2007). PCL-2, which contains 20 mg ZnO NPs-L, showed the highest swelling, reaching 57 800% at 120 min. The enhanced protonation of amino and carbonyl groups from the polymers, which improves the hydrophilicity of the polymer network, is related to increasing the swelling capacity with higher ZnO NPs-L concentrations (Zumbuehl et al. 2007). Biodegradable polymers are an outstanding source for the packaging of food; hydrogel-based materials can easily remove excess water and extend the shelf life of the food products (Batista et al. 2019). Hydrogels have excellent properties, and their three-dimensional structure easily retains and absorbs excess amounts of water (Niemczyk-Soczynska et al. 2023).

Hydrogel swelling in different buffer solutions. The swelling behaviour of hydrogels is a key indicator of their suitability for biomedical applications. In this study, to enhance the sensitivity of the polymeric chains to pH change, pH-responsive hydrogels were developed, with ZnO NPs-L incorporated. To assess the impact of pH on swelling capacity, the hydrogels were immersed in buffer solutions ranging from pH 2 to pH 10. As illustrated in Figure 11, all hydrogels (PC, PCL-1, and PCL-2) exhibited minimal swelling at pH 2, followed by a sharp increase at pH 4 and a subsequent decrease at neutral pH. In alkaline media, a slight increase in swelling was observed compared to acidic conditions. The swelling behaviour is influenced by the pKa values of its acidic groups and the pKb values of its basic pendant groups present in the hydrogels. The polymer network in this study comprises PT, which contains carboxyl groups that enhance pH responsiveness by protonating under acidic conditions and CS, with amino groups that protonate below pH 6, forming positively charged ammonium ions. Together, these biopolymers significantly influence the swelling behaviour of the hydrogels (Zumbuehl et al. 2007). As the pH increased, deprotonation of the amino groups took place, which led towards reduced electrostatic interactions between the polymer network and solvent, thereby reducing swelling (Booty et al. 2018).

At basic pH levels, enhanced deprotonation tends to limit the swelling of the hydrogels, often resulting in minimal or negligible expansion. The overall swelling trend of all hydrogels remained consistent across all hydrogel formulations, instead of the variations in environmental pH (Islam et al. 2023). However, the degree of swelling was influenced by the concentration of ZnO NPs-L. As the concentration of ZnO NPs-L increases, so does the swelling of the hydrogel. This is likely due to the increased number of protonation sites provided by ZnO NPs-L. Higher ZnO NPs-L concentrations lead to greater protonation, resulting in significant swelling in acidic media at pH 4 (Purkait et al. 2023).

Swelling in electrolytes. Swelling experiments were conducted in vitro by using different con-

https://doi.org/10.17221/159/2025-CJFS

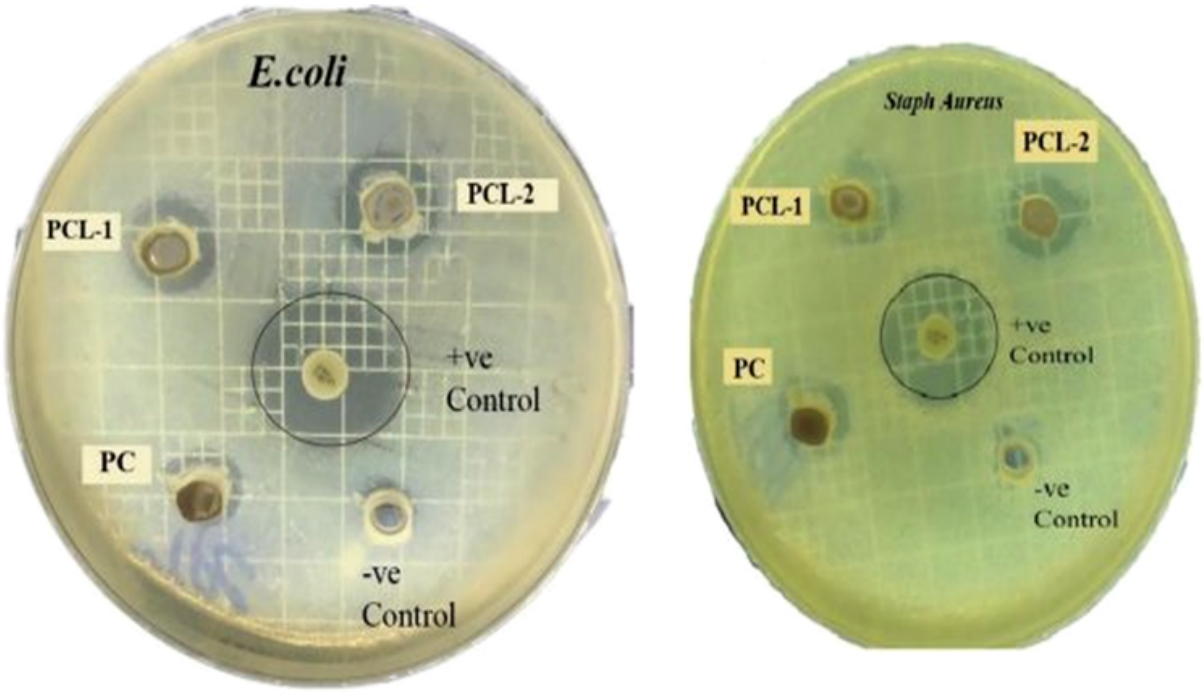

Figure 13. Antimicrobial zone of PT/CS based hydrogels: PC (without ZnO NPs-L), PCL-1 (with 10 mg ZnO NPs-L) and PCL-2 (with 20 mg ZnO NPs-L) against *E. coli* and *S. aureus* using standard antibiotic chloramphenicol as a positive control and DMSO as a negative control

PT – pectin; CS – chitosan; ZnO NPs-L – zinc oxide nanoparticles

centrations of molar solutions of NaCl and $CaCl_2$ to assess the impact of electrolytes such as Na, Ca, and Cl^- on the swelling properties of the hydrogels**.** The swelling pattern in both salts (NaCl and $CaCl_2$) showed that as the concentration of the salts increased, the swelling decreased. The findings of electrolyte-based swelling analysis of hydrogels are shown in Figures 12A and 12B. NaCl, with its monovalent Na^- cation, and $CaCl_2$, with its divalent Ca^{2+}, both share a common Cl^-. The reduction in swelling can be attributed to the charge screening effect of the ions (Shao et al. 2010). The swelling behaviour of hydrogels in $CaCl_2$ was reduced as compared to NaCl, which was likely due to the stronger screening effect of the divalent calcium cation.

Table 1. Diameter (mm) inhibition zones antimicrobial activity observed for hydrogels PC (without ZnO NPs-L), PC-1 (with 10 mg ZnO NPs-L), and PCL-2 (with 20 mg ZnO NPs-L) against *E. coli* and *S. aureus*

Bacteria strains	PC (mm)	PCL-1 (mm)	PCL-2 (mm)
E. coli	9 ± 0.15^c	13 ± 0.25^b	18 ± 0.30^a
S. aureus	8 ± 0.13^c	12 ± 0.20^b	16 ± 0.25^a

$^{a–c}$different letters indicate significant difference at $P \leq 0.05$; ZnO NPs-L – zinc oxide nanoparticles

Antibacterial activity

Figure 13 demonstrated the antimicrobial activity of PT/CS-based hydrogels against gram-positive bacteria *S. aureus* and gram-negative bacteria *E. coli.* The zones of inhibition surrounding each sample on the agar plate indicate the extent of bacterial growth suppression. The positive control, chloramphenicol (+ve control), showed a clear zone of inhibition, confirming its effectiveness against *E. coli* and *S. aureus* (Adigbli et al. 2016; Gila Vilchez et al. 2019). The negative control, DMSO (–ve control), did not exhibit any inhibition, indicating no antibacterial effect. As seen in Figure 13, all tested samples showed an inhibitory zone of bacterial growth against both bacterial strains, which can be attributed to the antibacterial properties of CS, PT and ZnO NPs-L combined within the structure of hydrogels. Among the hydrogels, PCL-2, with the highest concentration of ZnO NPs-L, displayed the largest inhibition zone (Table 1), suggesting that increasing the concentration of ZnO NPs-L enhanced the hydrogels' antibacterial properties. PCL-1 also showed a noticeable inhibition zone, although small-

https://doi.org/10.17221/159/2025-CJFS

er than PCL-2, while the PC hydrogel, which has no ZnO NPs-L, shows minimal antibacterial activity. This suggested that the incorporation of ZnO NPs-L is crucial for the antimicrobial effectiveness of these hydrogels. The antibacterial mechanism of ZnO-NPs-L is attributed to the release of Zn^{2+} ions, which contribute to the breakdown of lipids and proteins in bacterial cell membranes. Similar mechanisms have been proposed for the antibacterial mechanism of CS and PT (Hosoya et al. 2016; Kato and McKnight 2021). The NH^{3+} ions in the CS structure can bind with negatively charged ions on cell membranes, and COO^{-} can interact with the positively charged components of bacterial cell walls, resulting in cytoplasmic leakage into the extracellular matrix (Alsharbaty et al. 2024). ZnO-based hydrogel material as a biodegradable active packaging material in the preservation of food. They have good antimicrobial effects (*E. coli* and *S. aureus*), thereby increasing the shelf life of perishable foods, barrier properties, enhancing mechanical properties and UV-shielding properties (Cheang et al. 2025). Hydrogel-based biopolymer packaging enhanced its functionality by incorporating antimicrobial agents to remove reactive oxygen species and food spoilage.

CONCLUSION

PT/CS-based hydrogel samples were prepared by incorporating metallic nanoparticles, ZnO NPs-L, used as functional filler. The FTIR results confirmed the successful formation of nanoparticles and their effective interaction with the polymeric hydrogels. The SEM images and XRD investigation also confirmed the nanoscale dimension of the synthesised ZnO NPs-L. The swelling ratios of PT/CS films without or with 10 mg NPs were 4 140% and 5 000%, respectively; however, it increased up to 5 780% when 20 mg ZnO NPs-L were incorporated. The PCL-1 and PCL-2 hydrogels exhibited higher hydrophilicity, gel strength, thermal and mechanical and other properties than the control sample (PC). The PT/CS-based hydrogel with green-synthesised ZnO NPs-L exhibited strong antibacterial activity against pathogenic bacteria, *E. coli and S. aureus*. The research work done supports the core objective of the present study, which was to develop a novel green nanocomposite hydrogel with enhanced properties to fill the gap in both the biomedical and agricultural sectors. The developed nanocomposite hydrogels, especially PCL-2, have great potential for application in different fields of interest due to better mechanical, swelling and antimicrobial properties.

Acknowledgement. The authors are thankful to the Department of Nutritional Sciences, Govt. College University Faisalabad, Pakistan, for providing us with the facilities to carry out this work. Furthermore, we are also grateful to Ms. Saba Urooge, Institute of Polymer and Textile Engineering, University of Punjab, Pakistan, for facilitating some research work part over there.

REFERENCES

Adigbli G., Alshomer F., Maksimcuka J., Ghali S. (2016): Principles of plastic surgery, wound healing, skin grafts and flaps. In: Kalaskar D.M., Butler P.E., Ghali S. (eds): Textbook of Plastic and Reconstructive Surgery. London, UCL Press: 3–37.

Ahmad A., Reddy S.S. (2020): Performance evaluation of upflow anaerobic sludge blanket reactor using immobilised ZnO nanoparticle enhanced continuous biogas production. Energy Environment, 31: 330–347.

Alameen A.S., Undre S.B., Undre P.B. (2024): Synthesis, dispersion, functionalization, biological and antioxidant activity of metal oxide nanoparticles. Nano-Structures & Nano-Objects, 39: 101298.

Alsharbaty M.H.M., Naji G.A., Ghani B.A., Schagerl M., Khalil M.A., Ali S.S. (2024): Cytotoxicity and antibacterial susceptibility assessment of a newly developed pectin–chitosan polyelectrolyte composite for dental implants. Scientific Reports, 14: 16968.

Aziz A.A., Shaniba V.S., Jayasree P.R., Kumar P.M. (2019): Physico-chemical, photocatalytic and cytotoxicity evaluation of *Annona muricata* L. fruit extract derived zinc oxide nanoparticles in comparison to the commercial chemical version. Current Science, 117: 1492–1504.

Batista R.A., Espitia P.J.P., Quintans J.D.S.S., Freitas M.M., Cerqueira M.Â., Teixeira J.A., Cardoso J.C. (2019): Hydrogel as an alternative structure for food packaging systems. Carbohydrate Polymers, 205: 106–116.

Bhavikatti A.S., Furtado S.C., Mallya P., Basavaraj B.V. (2025): A review of natural polymer based biomaterials for wound care: Addressing challenges and future perspectives. Journal of Biomaterials Science, Polymer Edition, 379: 93–117.

Booty S.J., Harding D.R., Whitby C.P., Gater M., Chambers P., Singh P.M. (2018): Sustained-release injectable hydrogel formulations for administration of sodium salicylate in broiler chickens. Journal of Avian Medicine and Surgery, 32: 294–300.

Boura-Theodoridou O., Giannakas A., Katapodis P., Stamatis H., Ladavos A. Barkoula N.M. (2020): Performance of ZnO/chitosan nanocomposite films for antimicrobial packaging applications as a function of NaOH treatment

https://doi.org/10.17221/159/2025-CJFS

and glycerol/PVOH blending. Food Packaging and Shelf Life, 23: 100456.

Cao Y., Bolisetty S., Wolfisberg G., Adamcik **J**., Mezzenga R. (2019): Amyloid fibril-directed synthesis of silica core–shell nanofilaments, gels, and aerogels. Proceedings of National Academy of Sciences, 116: 4012–4017

Cheang W.H., Yu T.C., Wang Y.J., Yang J.S., Wu P.W. (2025): Electrophoretic synthesis of composite hydrogels chitosan polyethylene glycol ZnO_2 and their characterization for food-packaging applications. Electrochemical Society Meeting Abstracts, MA2025-02: 1363–1363.

Dessislava M., Veselin I. (2020): Micro-macro transition for numerical simulation of submerged membrane bioreactor. The EuroBiotech Journal, 4: 1457–1536.

Diez-Pascual A.M., Diez-Vicente A.L. (2014): High-performance aminated poly(phenylene sulfide)/ZnO nanocomposites for medical applications. ACS Applied Materials & Interfaces, 6: 10132–10145.

Dimitrou P., Castell O., Birchall J., Li J. (2024): Label-free volumetric imaging of synthetic cell chassis using optical coherence tomography. In: Spezi E., Bray M. (eds): Proceedings of Cardiff University Engineering Research Conference 2023. Cardiff, July 12–14, 2023: 15–18.

Dzulkharnien N.S.F., Rohani R., Radzuan H.A. (2024): Comparative analysis: Particle size and bactericidal efficacy of zinc oxide nanoparticles with aloe vera gel versus aloe vera gel-honey. Physica Scripta, 99: **0**85030.

Ebrahimi A.K., Barani M., Sheikhshoaie I. (2018): Fabrication of a new superparamagnetic metal-organic framework with core-shell nanocomposite structures: Characterization, biocompatibility, and drug release study. Materials Science and Engineering: C, 92: 349–355.

Fu F., Chen Z., Zhao Z., Wang H., Shang L., Gu Z., Zhao Y. (2017): Bio-inspired self-healing structural color hydrogel. Proceedings of the National Academy of Sciences, 114: 5900–5905.

Gila-Vilchez C., Manas Torres M.C., Contreras Montoya R., Alaminos M., Duran J.D., de Cienfuegos L.Á., Lopez-Lopez M.T. (2019): Anisotropic magnetic hydrogels: Design, structure and mechanical properties. Philosophical Transactions of the Royal Society A, 377: 20180217.

Gojova, A., Guo, B., Kota, R.S., Rutledge, J.C., Kennedy, I.M. Barakat, A.I. (2007): Induction of inflammation in vascular endothelial cells by metal oxide nanoparticles: Effect of particle composition. Environmental Health Perspectives, 115: 403–409.

He C., Zhao Y., Wang F., Oh K., Zhao Z., Wu C., Li X. (2020): Phytoremediation of soil heavy metals Cd and Zn by castor seedlings: Tolerance, accumulation and subcellular distribution. Chemosphere, 252: 126471.

Hosoya H., Dobroff A.S., Driessen W.H.P., Cristini V., Brinker L.M., Staquicini F.I., Cardó-Vila M., D'Angelo S., Ferrara F., Proneth B., Lin Y.S., Dunphy D.R., Dogra P., Melancon M.P., Stafford R.J., Miyazono K., Gelovani J.G., Kataoka K., Brinker C.J., Sidman R.L., Arap W., Pasqualini R. (2016): Integrated nanotechnology platform for tumor-targeted multimodal imaging and therapeutic cargo release. Proceedings of the National Academy of Sciences, 113: 1877–1882.

Hua B., Xiong H., Kadhom M., Wang L., Zhu G., Yang J., Cunningham G., Deng B. (2017): Physico-chemical processes. Water Environment Research, 89: 974–1028.

Islam M.M., Ahmed F., Mondal M.I.H. (2023): Development of methylcellulose/polyvinylpyrrolidone nanocomposites enriched with biogenic zinc oxide nanoparticles for wound healing applications. Biomedical: Journal of Scientific & Technical Research, 49: 40624–40633.

Kamanna K., Amaregouda Y., Kumar M. (2023): Chitosan/polyvinyl alcohol-based nanocomposite films incorporated with L-Glu surface functionalized ZnO NPs: Physicochemical, photocatalytic, antimicrobial and antioxidant properties evaluation. Environmental Nanotechnology, Monitoring & Management, 20: 100861.

Karanth S., Feng S., Patra D., Pradhan A.K. (2023): Linking microbial contamination to food spoilage and food waste: The role of smart packaging, spoilage risk assessments, and date labelling. Frontiers in Microbiology, 14: 1198124.

Kato M., McKnight S.L. (2021): The low-complexity domain of the FUS RNA binding protein self-assembles via the mutually exclusive use of two distinct cross-β cores. Proceedings of the National Academy of Sciences, 118: e2114412118.

Kaur S., Bains K. (2023): *Aloe barbadensis* Miller (*Aloe vera)*. International Journal of Vitamin and Nutrition Research, 94: 308–321.

Ko H.F., Sfeir C., Kumta P.N. (2010): Novel synthesis strategies for natural polymer and composite biomaterials as potential scaffolds for tissue engineering. Philosophical Transactions of the Royal Society A, 368: 1981–1997.

Kumar S., Prasad M., Rao R. (2021): Topical delivery of clobetasol propionate loaded nanosponge hydrogel for effective treatment of psoriasis: Formulation, physicochemical characterization, antipsoriatic potential and biochemical estimation. Materials Science and Engineering, 119: 111605.

Lee D.K., Kee T., Liang Z., Hsiou D., Miya D., Wu B., Osawa E., Chow E.K.H., Sung E.C., Kang M.K., Ho D. (2017): Clinical validation of a nanodiamond-embedded thermoplastic biomaterial. Proceedings of the National Academy of Sciences, 114: E9445–E9454.

Li M., Mahmudov R., Huang C.P. (2010): Hazardous waste treatment technologies. Water Environmental Resources, 82: 1720–1747.

https://doi.org/10.17221/159/2025-CJFS

Li C., Wang P., Lombi E., Wu J., Blamey F.P.C., Fernández V., Howard D.L., Menzies N.W., Kopittke P.M. (2018): Absorption of foliar applied Zn is decreased in Zn deficient sunflower (*Helianthus annuus*) due to changes in leaf properties. Plant and Soil, 433: 309–322.

Mahendiran D., Subash G., Arumai Selvan D., Rehana D., Senthil Kumar R., Kalilur Rahiman A. (2017): Biosynthesis of zinc oxide nanoparticles using plant extracts of *Aloe vera* and *Hibiscus sabdariffa*: Phytochemical, antibacterial, antioxidant, and anti-proliferative studies. BioNanoScience, 7: 530–545.

Meji M.A., Usha D., Sankar M.H., Ashwin B.M. (2023): Synthesis of ZnO nanoparticles from zinc acetate dihydrate – An environmentally friendly technique. Materials Today: Proceedings.

Momoh J.O., Kumar S., Olaleye O.N., Adekunle O.M., Aiyelero T.S. (2024): Green synthesis of characterized bio-functionalized ZnO nanoparticles from *Terminalia catappa* (almond) methanol leaf extract and their potential antioxidant and antibacterial properties. Tropical Journal of Natural Product Research, 8: 9296–9309.

Multanen V., Bhushan B. (2019): Bioinspired self-healing, super liquiphobic and self-cleaning hydrogel-coated surfaces with high durability. Philosophical Transactions of the Royal Society A, 377: 20190117.

Nejatzadeh-Barandozi F. (2013): Antibacterial activities and antioxidant capacity of *Aloe vera*. Organic and Medicinal Chemistry Letters, 3: 5.

Ngo C., Natowitz J.B. (2017): Nanomaterials and nanostructures. In: Natowitz J.B., Ngo C. (eds): Our Nanotechnology Future. Amsterdam, Amsterdam University Press: 49–60.

Niemczyk-Soczzyńska B., Kolbuk D., Mikułowski G., Ciechomska I.A., Sajkiewicz P. (2023): Methylcellulose/agarose hydrogel loaded with short electrospun PLLA/laminin fibers as an injectable scaffold for tissue engineering/3D cell culture model for tumour therapies. RSC Advances, 13: 11889–11902.

Pathan S., Bose S. (2020): Biopolymer based hydrogels for arsenic removal. Current Science, 118: 1540–1546.

Pellegrin M.L., Min K., Diamond J., Sadler M.E., Greiner A.D., Zhang K., Aguinaldo J., Arabi S., Liu M., Burbano M.S., Padhye L.P., Kent F., McCandless R. (2014): Membrane processes. Water Environment Research, 86: 1101–1197.

Phadke A., Zhang C., Arman B., Hsu C.C., Mashelkar R.A., Lele A.K., Tauber M.J., Arya G., Varghese S. (2012): Rapid self-healing hydrogels. Proceedings of the National Academy of Sciences, 109: 4383–4388.

Pires J.R.A., Rodrigues C., Coelhoso I., Fernando A.L., Souza V.G.L. (2023): Current applications of bio nanocomposites in food processing and packaging. Polymers: 15: 2336.

Popa L., Ghica M.V., Dinu-Pîrvu C.E., Dumitrescu I.A. (2025): Chitosan-pectin composite biomaterials: Types, interactions, formulations, and biomedical in chitosan and alginate. In: Popa L., Azad M.A.K., Ghica M.V., Dinu-Pîrvu C.E., Hudita A., Miret M.M. (eds): Chitosan and Alginate Frontiers – Innovations and Applications in Life Sciences, Food, and Industry. London, IntechOpen: 59–83.

Pourjavadi A., Barzegar S., Zeidabadi F. (2015): Synthesis and characterization of antibacterial carboxymethyl cellulose/ZnO nanocomposite hydrogels. International Journal of Biological Macromolecules, 75: 222–229.

Pourrezaei P., Afzal A., Ding N., Islam M.S., Moustafa A., Drzewicz P.Ł., Chelme-Ayala P., El-Din M.G. (2010): Physico-Chemical Processes. Water Environment Research, 82: 997–1072.

Purkait P., Bhattacharyya A., Roy S., Maitra S., Das G.C., Ghosh Chaudhuri M. (2023): Green synthesis of ZnO nanoparticle using *Trema orientalis* (L) leaf: An efficient photocatalyst for degradation of zoxamide fungicide in aqueous organic media under UV light irradiation. International Journal of Environmental Analytical Chemistry, 103: 307–325.

Qureshi M.A.R., Arshad N., Rasool A., Islam A., Rizwan M., Haseeb M., Rasheed T., Bilal M. (2024): Chitosan and carrageenan-based biocompatible hydrogel platforms for cosmeceutical, drug delivery, and biomedical applications. Starch, 76: 2200052.

Rastegari A., Hasanshakir F., Mohammadi Z., Saadatpour F., Faghihi H., Moraffah F. (2023): A chitosan-based hydrogel containing zinc oxide nanoparticles as a carrier for improving antibacterial activity and controlling the release of antibiotics. Micro & Nano Letters, 18: e12172.

Rata D.M., Cadinoiu A.N., Daraba O.M., Gradinaru L.M., Atanase L.I., Ichim D.L. (2023): Influence of ZnO nanoparticles on the properties of ibuprofen-loaded alginate-based biocomposite hydrogels with potential antimicrobial and anti-inflammatory effects. Pharmaceutics, 15: 2240.

Read M.L., Morgan P.B., Kelly J.M., Maldonado-Codina C. (2011): Dynamic contact angle analysis of silicone hydrogel contact lenses. Journal of Biomaterials Applications, 26: 85–99.

Rhodes C.J. (2015): Sustainable nanotechnology. Science Progress, 98: 63–72.

Sabbagh F., Khatir N.M., Kiarostami K. (2023): Synthesis and characterization of κ-carrageenan/PVA nanocomposite hydrogels in combination with MgZnO nanoparticles to evaluate the catechin release. Polymers, 15: 272.

Seliktar D. (2012): Designing cell-compatible hydrogels for biomedical applications. Science, 336: 1124–1128.

Shao Y., Quyang L., Zhou Y., Tang J., Tan Y., Liu Q., Lin Z., Yin T., Qiu F., Liu Z. (2010): Preparation and physical properties of a novel biocompatible porcine corneal acellularized matrix. In Vitro Cellular & Developmental Biology – Animal, 46: 600–605.

https://doi.org/10.17221/159/2025-CJFS

Singh S., Dodiya T.R., Singh S., Dodiya R. (2021): Topical wound healing, antimicrobial and antioxidant potential of *Mimosa pudica* Linn root extracted using *n*-hexane followed by methanol, fortified in ointment base. International Journal of Pharmaceutical Sciences and Nanotechnology, 14: 5472–5480.

Smeraldi J., Ganesh R., Hosseini T., Khatib L., Olson B.H., Rosso D. (2017): Fate and toxicity of zinc oxide nanomaterial in municipal wastewaters. Water Environment Research, 89: 880–889.

Tian X., Zhu H., Meng X., Wang J., Zheng C., Xia Y., Xiong Z. (2020): Amphiphilic calcium alginate carbon aerogels: Broad-spectrum adsorbents for ionic and solvent dyes with multiple functions for decolorized oil–water separation. ACS Sustainable Chemistry & Engineering, 8: 12755–12767.

Wang Y., Huang W., Wang Y., Mu X., Ling S., Yu H., Chen W., Guo C., Watson M.C., Yu Y., Black III L.D., Li M., Omenetto F.G., Li C., Kaplan D.L. (2020): Stimuli-responsive composite biopolymer actuators with selective spatial deformation behavior. Proceedings of National Academy of Sciences, 117: 14602–14608.

Xue B., Tang D., Wu X., Xu Z., Gu J., Han Y., Zhu Z., Qin M., Zou X., Wang W., Cao Y. (2021): Engineering hydrogels with homogeneous mechanical properties for controlling stem cell lineage specification. Proceedings of National Academy of Sciences, 118: e2110961118.

Yadav M., Das M., Thakore S., Jadeja R.N. (2022): Role of biopolymers in development of sustainable remediation technologies. In: Singh P., Hussain C.M., Sillanpää M. (eds): Innovative Bio-Based Technologies for Environmental Remediation. Boca Raton, CRC Press: 295–319.

Youssef A.M., El-Sayed S.M. (2018): Bionanocomposites materials for food packaging applications: Concepts and future outlook. Carbohydrate Polymers, 193: 19–27.

Zhao Z., Kumar J., Hwang Y., Deng J., Ibrahim M.S.B., Huang C., Suresh S., Cho N.J. (2021): Digital printing of shape-morphing natural materials. Proceedings of National Academy of Sciences, 118: **e**2113715118.

Zumbuehl A., Ferreira L., Kuhn D., Astashkina A., Long L., Yeo Y., Iaconis T., Ghannoum M., Fink G.R., Langer R., Kohane D.S. (2007): Antifungal hydrogels. Proceedings of the National Academy of Sciences, 104: 12994–12998.

Received: August 20, 2025
Accepted: June 11, 2026
Published online: July 17, 2026